Water Research X 13 (2021) 100121

Contents lists available at ScienceDirect

Water Research X

journal homepage: www.sciencedirect.com/journal/water-research-x

Predictability of initial hydrogeochemical effects induced by short-term infiltration of ~75 °C hot water into a shallow glaciogenic aquifer

Klas Lüders *, Götz Hornbruch, Nilufar Zarrabi, Stefan Heldt, Andreas Dahmke, Ralf Köber

Institute of Geosciences - Kiel University

ARTICLE INFO

Keywords:
Underground thermal energy storage
Groundwater quality
Hot water infiltration field test
Batch test based prognosis
Hydrogeochemical predictability

ABSTRACT

Despite their potential in heating supply systems, thus far high-temperature aquifer thermal energy storages (HT-ATES) currently lack widespread application. Reducing the potential risks by improving the predictability of hydrogeochemical processes accelerated or initiated at elevated temperatures might promote the development of this technology. Therefore, we report the results of a short-term hot water infiltration field test with subsurface temperatures above 70 °C, along with associated laboratory batch tests at 10, 40 and 70 °C for 28 sediment samples to determine their usability for geochemical prediction.

Most groundwater components had lower maximal concentrations and smaller concentration ranges in field samples compared to the batch tests. This indicates that the strongest geochemical effects observed in laboratory tests with sufficient site-specific sediment samples will likely be attenuated at the field scale. A comparison of field measurements with predicted concentration ranges, based on temperature induced relative concentration changes from the batch tests, revealed that the predictive power was greatest, where the hot infiltrated water had cooled least and the strongest geochemical effects occurred. The batch test-based predictions showed the best accordance with field data for components, with significant temperature-induced concentration changes related to ion exchange and (de)sorption processes. However, accurate prediction of concentration changes based on other processes, e.g. mineral dissolution, and downstream reversals in concentrations, requires further investigation.

The here presented procedure enables the prediction of maximal expectable temperature-dependant concentration changes for most environmentally relevant ancillary groundwater components, e.g. As, with limited effort.

1. Introduction

Seasonal high-temperature aquifer thermal energy storages (HT-ATES) in urban areas have the potential to be a key technology in the transformation of the heating sector energy system away from the use of fossil fuels (Henning and Palzer, 2012). However, thus far, the wider application of ATES systems with temperatures above 50 °C has been hampered by technical, financial, social, political and legal risks (Fleuchaus et al., 2020). One aspect, that causes potential technical or legal issues, is the various hydrogeochemical processes accelerated or initiated by elevated temperatures of up to 90 °C, and the induced changes to the flow regime (Bauer et al., 2013; Jenne et al., 1992).

This includes processes associated with operational issues, such as i) accelerated corrosion (Andersson, 1990; Jenne et al., 1992); ii) the precipitation of carbonates (Griffioen and Appelo, 1993) and Fe and Mn (hydr)oxides (Andersson, 1990; Willemsen, 1990) that can cause scaling within heat exchangers, pipes and in and around wells; iii) the formation of a separate gas phase (Lüders et al., 2016) that can block pipes or parts of the near-well pore space and iv) the dissolution of amorphous silica and silicates at increased temperatures (Arning et al., 2006; M. Bonte et al., 2013b; Holm et al., 1987) that can precipitate when the water is cooled in the surface installations during heat recovery (Gunnarsson and Arnórsson, 2005). There are also processes associated with potential changes in groundwater quality, such as i) the release of dissolved organic carbon (DOC) and associated redox processes (Bonte et al., 2013a; Brons et al., 1991; Jesußek et al., 2013a; 2013b); ii) the release and fixation of trace elements and heavy metals (M. Bonte et al., 2013b; García-Gil et al., 2016; Lüders et al., 2020; Saito et al., 2016) and iii) increased or decreased solubility (Koproch et al., 2019), volatilisation (Schwardt et al., 2021) and degradation (Men and Cheng, 2011;

* Corresponding author.
E-mail address: klas.lueders@ifg.uni-kiel.de (K. Lüders).

https://doi.org/10.1016/j.wroa.2021.100121
Received 12 April 2021; Received in revised form 14 September 2021; Accepted 17 September 2021
Available online 23 September 2021

Němeček et al., 2018; Zuurbier et al., 2013) of organic contaminants.

These hydrogeochemical processes have been investigated in laboratory studies using batch (Arning et al., 2006; Jesußek et al., 2013a; Koproch et al., 2019; Men and Cheng, 2011; Schwardt et al., 2021), flow-through (Bonte et al., 2013a; M. 2013b; Griffioen and Appelo, 1993; Jesußek et al., 2013a; 2013b; Lüders et al., 2016) and circular flow column tests (Lüders et al., 2020). Furthermore, attempts have been made to empirically categorise trace elements and heavy metals relevant for administrative approval (Lüders et al., 2020). Previous HT-ATES field tests, installed in depths varying from below 10 to above 200 m below ground surface (bgs), have mainly focussed only on processes that potentially damage the ATES operation itself, as well as on technical solutions to prevent these processes (Andersson, 1990; Jenne et al., 1992; Molz et al., 1981; Opel et al., 2014; Perlinger et al., 1987; Ueckert and Baumann, 2019). Initial hydrogeochemical effects with potential environmental consequences relevant for administrative approval (Bonte et al., 2011; Hähnlein et al., 2013; Possemiers et al., 2014) and observations of geochemical effects downstream of the infiltration well have not been in focus of HT-ATES field tests so far. Furthermore, all the aforementioned studies focus either on laboratory investigations or on field observations. Thus, whether laboratory investigations with site material and water can yield reliable predictions regarding temperature-dependent (initial) hydrogeochemical effects at the aquifer scale is largely undetermined.

Therefore, this work combines a short-term hot water infiltration field test with temperatures of up to 78 °C, with preceding laboratory batch tests for 28 sediment samples from the field test site. Essential questions investigated by this approach include:

- Which initial component-specific, temperature-dependent geochemical effects observed in the hot water infiltration field test can be predicted by the laboratory investigations, and to what extent?
- How does the geochemical heterogeneity of the sediments affect variances in geochemical behaviour at the laboratory and field scale?

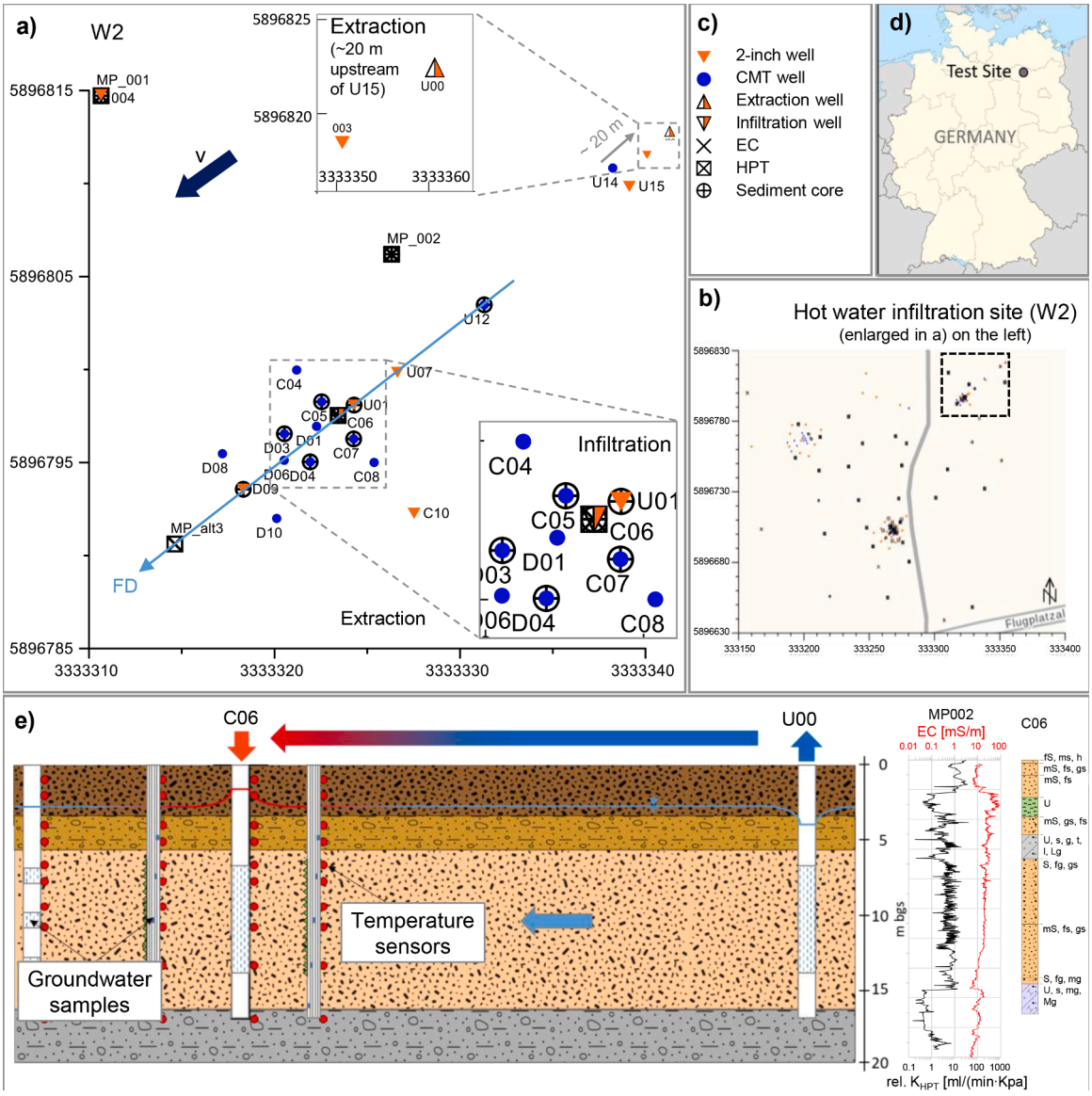

Fig. 1. Monitoring network of the hot water infiltration field test site (a; profile FD is used in Fig. 3 for illustrating temperature changes) and the wider TestUM field test area with the framed hot water infiltration site (b); the respective legend (c); the location of the TestUM field test site (d); and a simplified subsurface structure and test setup along a selection of hydraulic-profiling tool (HPT), electrical conductivity (EC) and drill log exploration data (e; data curve colours are equal to the axis label); partly from Heldt et al., 2021 and Keller et al., 2021.

2. Materials and methods

2.1. "TestUM" field test site

The "TestUM" field test site is located near Wittstock, Brandenburg, Germany [53°11′40″N, 12°30′18″E], on an abandoned airfield. Subsurface exploration during an earlier CO_2 injection test on the same site, a few metres away (Peter et al., 2012), showed that the shallow subsurface consists of typical northern German glacio-fluviatile Quaternary sediments, with alternating layers of sandy and cohesive sediments of variable thickness. Based on further drill logs and geophysical investigation with an electric conductivity (EC) and a hydraulic-profiling-tool (HPT), an area featuring a ~9 m thick sandy layer, 6–15 m bgs, overlaid by a 2–3 m thick cohesive layer was chosen for the hot water infiltration test (see also Heldt et al., 2021; Keller et al., 2021). Groundwater head measurements between 2.9 and 3.5 m bgs showed that the sandy layer used for infiltration is confined. Locally, groundwater flowed in west-southwest direction, with a mean hydraulic gradient of 0.0011 and a mean groundwater flow velocity of 0.09 m/d (Heldt et al., 2021).

For setting up the test field, one 2″ extraction and one 2″ infiltration well screened in 7 – 14 m bgs, five 2″ monitoring wells each screened at 7–8, 10–11 and 13–14 m bgs and 12 multi-level CMT®-wells (Continuous Multichannel Tubing; Solinst Canada Ltd., Georgetown, Ontario, CA) screened at 5 (partial), 7.5, 10.5, 13.5 and 17 m bgs were installed with sonic drilling (see Fig. 1 for a map of the field tests monitoring network). This resulted in 71 groundwater-monitoring points distributed over 17 wells.

2.2. Laboratory experiments

2.2.1. Sediment and water procurement and characterisation

Before installing the monitoring wells, ~100 kg of sediment samples from 0 to 18 m bgs were obtained from nine different bore holes (at positions U01, U12, C05, C06, C07, D03, D04, D09 and MP002; Fig. 1) by either macro-core® or sonic drilling (Geoprobe Systems®, Salina, Kansas, US). Macro-core® drilling yields sediment samples with minimal physical and chemical disturbance (EPA, 1997), in contrast, sonic drilling can cause elevated temperatures at the drill core interface and thus might potentially affect temperature dependent geochemical behaviour in subsequent laboratory investigations. However, there were no noticeable deviations in the temperature-induced geochemical effects of the different sediment samples depending on the used drilling technique, wherefore no further differentiation regarding the drilling technique was made. Each half-metre drill core, consisting of, on average, 1733 g sediment, was mixed and split into three parts: 1) a 400 g individual sediment sample, specific to the respective well location and half metre depth range; 2) half of the remaining sediment was mixed to a homogenised composite sample of the infiltration layer and 3) the rest was kept in the drill cores as backup material. The individual sediment samples were used to investigate the heterogeneity in hydrogeochemical behaviour at elevated temperatures. The homogenised composite sample of the infiltration layer was used for geochemical characterisation (with triplicates, Table 1) and for further laboratory investigations with a higher sediment demand not part of this study. All sediment samples were stored under argon atmosphere in refrigerators at 10 °C until further use. The water used for the laboratory experiments was repeatedly pumped from the extraction well and well 004 (Fig. 1) and stored at 10 °C in a refrigerator in gas-tight bags (PET/Al/-PE-composite) to avoid gas exchange with the atmosphere (Table 2).

Sediment samples from the same wells, but from the low permeable layers above and below the target aquifer utilised for the hot water infiltration have been investigated in a separate study (Meier zu Beerentrup and Dahmke, 2021).

2.2.2. Batch tests

Batch tests were used to determine the heterogeneity in hydrogeochemical behaviour of individual sediment samples at elevated temperatures and to consider the observed variance for the subsequent predictive calculations (Section 2.5), due to their low sample volume requirements. Sediment samples ($n = 28$), from the sandy aquifer section into which the hot water was infiltrated (6–15 m bgs), were tempered for one week at 60 rpm in a shaking chamber to 10 and 40 °C, and in a custom build heating chamber on a shaker to 70 °C. For each of the 84 batches, 40 g of sediment and 80 mL of site water were filled into 200 mL HDPE vials (sediment samples from C, D and U wells, with site water from extraction well U00) or 100 mL glass vials (sediment samples from MP002 drill core, with site water from well 004) in an argon filled glove box (Table 2), to avoid oxygen intrusion. The vials were closed with HDPE screw caps or aluminium crimp caps with butyl septa, respectively. The potential degassing of CO_2 while filling the vials cannot be prevented with this procedure. To identify concentration changes induced by the vial material, blank tests with both vial materials and site water, but without sediment, were applied at each temperature (see Table A.3 in the supplementary material). Due to the high ratio between the concentrations resulting from the releases from the blank vials versus the respective mean concentration increase in the sediment batch tests for Si_{diss} with the glass vials (up to 1.31) and non-purgeable organic carbon (NPOC) with the HDPE vials (up to 0.81), only the data from the sediment batch tests with the other vial material were used for further data evaluation for these two components. After one week, the vials were reopened and the water was separated from the sediment using 7 µm cellulose round filters, and then filled into the analytical vials (Section 2.4).

Table 1
Sediment characteristics of the target aquifer for the hot water infiltration test. Data of the different carbon and iron contents for the individual sediment samples, as well as data of the individual trace elements and heavy metals that are ionically bound are included in the supplementary material (Table A.1 and A.2, respectively).

	Composite sample
Sediment	Pleistocene sand
Extraction depth *[metres below ground surface]*	6–14
Grain fraction d60 *[µm]****; d10*** *[µm]****; d60/d10***	347 ± 69; 117 ± 40; 3.3 ± 1.0
silt *[%]****; sand*** *[%]****; gravel*** *[%]*	11 ± 8; 86 ± 8; 3 ± 3
C[1] *[mg/kg]*	1035 ± 225
$C_{org.}$[1] *[mg/kg]*	560 ± 265
$C_{carb.}$[1] *[mg/kg]*	517 ± 306
reactive Fe[2] *[mg/kg]*	407 ± 38
Fe bound in crystalline iron oxides, siderite and magnetite[3] *[mg/kg]*	1032 ± 245
$\sum$ ***ionically bound trace elements and heavy metals (listed in Section 2.4)***[4] *[mg/kg]*	65 ± 22

[1] determined with a Multi N/C 2100 Analyser with HT-1300 oven (Analytik Jena AG, Jena, Germany); total carbon (C) directly, total organic carbon ($C_{org.}$) after removal of total inorganic carbon ($C_{carb.}$) with 2 M HCL, $C_{carb.}$ was calculated from the difference between C and $C_{org.}$.

[2] determined by extraction with 1 M HCL according to Leventhal and Taylor (1990) and subsequent photometric analysis of the extracts according to the ferrozine method (Stookey, 1970) with hydroxylammonium chloride as the reductive agent.

[3] determined by extraction with 5 M HCL according to Heron et al. (1994) and subsequent photometric analysis of the extracts according to the ferrozine method (Stookey, 1970) with hydroxylammonium chloride as the reductive agent.

[4] determined by digestion with 1 M sodium dihydrogen phosphate at pH 5 adjusted with sodium hydroxide following the procedure described in Keon et al. (2001).

2.3. Short-term hot water infiltration field test

To identify the geochemical effects of elevated temperatures, the initial hydrogeochemical state and natural variations in the target

Table 2
Initial composition of the water used for laboratory experiments.

		site water from extraction well U00	*site water from well 004*
pH	[-]	6.24 ± 0.27	6.48 ± 0.18
O_2	*[mg/L]*	1.12 ± 0.36	2.66 ± 0.98
electrical conductivity	*[µS/cm]*	535 ± 2	427 ± 17
redox potential	*[mV]*	355 ± 235	373 ± 9
alkalinity	*[mmol/L]*	2.39 ± 0.29	–
NPOC	*[mg/L]*	2.89 ± 0.61	3.13 ± 1.27
TIC	*[mg/L]*	–	30.2 ± 5.1
K^+	*[mg/L]*	2.12 ± 0.38	1.30 ± 0.14
Na^+	*[mg/L]*	19.2 ± 1.2	9.80 ± 0.30
Ca^{2+}	*[mg/L]*	91.8 ± 5.9	75.3 ± 3.2
Mg^{2+}	*[mg/L]*	5.62 ± 0.22	5.06 ± 0.17
Fe_{diss}	*[µg/L]*	30.4 ± 17.9	43.7 ± 75.3
Mn_{diss}	*[µg/L]*	76.0 ± 9.5	2.97 ± 0.93
Si_{diss}	*[mg/L]*	4.88 ± 0.10	4.67 ± 0.12
Al_{diss}	*[µg/L]*	8.16 ± 4.17	6.17 ± 3.05
Cl^-	*[mg/L]*	9.05 ± 2.34	3.69 ± 0.42
NO_2^-	*[mg/L]*	<0.4	<0.2
NO_3^-	*[mg/L]*	6.67 ± 3.31	7.28 ± 0.81
SO_4^{2-}	*[mg/L]*	143 ± 18	100 ± 8
CH_4	*[µg/L]*	4.04 ± 1.77	0.60 ± 0.22
TCE	*[µg/L]*	5.51 ± 1.94	6.92 ± 2.05
Li	*[µg/L]*	1.64 ± 0.39	0.72 ± 0.05
V	*[µg/L]*	0.90 ± 0.22	0.68 ± 0.06
Cr	*[µg/L]*	0.12 ± 0.05	0.19 ± 0.07
Co	*[µg/L]*	0.79 ± 0.26	0.77 ± 0.69
Ni	*[µg/L]*	3.14 ± 1.60	2.17 ± 0.37
Cu	*[µg/L]*	2.71 ± 1.83	3.45 ± 1.84
Zn	*[µg/L]*	23.2 ± 10.2	29.1 ± 24.3
As	*[µg/L]*	0.29 ± 0.11	0.16 ± 0.01
Se	*[µg/L]*	0.48 ± 0.07	0.20 ± 0.10
Sr	*[µg/L]*	204 ± 7	164 ± 7
Mo	*[µg/L]*	0.22 ± 0.09	0.12 ± 0.04
Cd	*[µg/L]*	0.41 ± 0.15	0.09 ± 0.01
Sn	*[µg/L]*	0.012 ± 0.005	0.009 ± 0.005
Sb	*[µg/L]*	0.157 ± 0.016	0.039 ± 0.003
Ba	*[µg/L]*	61.8 ± 10.0	29.0 ± 0.5
Tl	*[µg/L]*	0.012 ± 0.002	0.005 ± 0.001
Pb	*[µg/L]*	0.274 ± 0.299	0.184 ± 0.076
U	*[µg/L]*	1.47 ± 1.13	0.091 ± 0.010

aquifer were characterised in six baseline sampling campaigns, conducted between October 2018 and April 2019 (224, 183, 128, 93, 64 and 28 days before the start of the hot water infiltration; Fig. A.1). Over the whole monitoring period from autumn 2018 to summer 2019, the groundwater heads increased by up to 40 cm, similarly in all the different monitoring wells. Thus, there are no indications for significant changes in the hydraulic gradient or the groundwater flow direction over time.

Hot water infiltration started on the 23rd of May 2019 and finished on the 29th of May 2019. A submersible pump pumped cold water from extraction well U00 into a cold-water buffer tank. There, the water was covered with argon to avoid oxygen intrusion; however, concomitant equilibration of CO_2 between the water phase and the argon coverage may have facilitated subsequent carbonate precipitation at elevated temperatures. From the cold-water buffer tank, the water was pumped through a plate heat exchanger, where it was heated to approximately 85 °C, then into a hot water buffer tank where the hot water could degas to minimise potential tube or well clogging by gas bubbles. To eliminate traces of the organic contaminant trichloroethylene (TCE; Table 2, Fig. A.1), the formed gas phase was dissipated over an activated carbon filter before being released. From the hot water buffer tank, the water flowed by gravity at ~14.5 L/min into the infiltration well. Towards the end of the hot water infiltration, the infiltration rate decreased to below 1 L/min (see Heldt et al., 2021), presumably due to clogging of tubes and the well screen caused by a combination of transported fines from the extraction well, precipitates and gas bubbles. In total, ~86 m^3 of ~75 °C hot water was infiltrated over a period of 4.5 days. Water extraction and infiltration superimposed the natural hydraulic conditions around the respective wells during operation, but the induced hydraulic signal faded away within a few hours (data not shown).

Subsequently, eight sampling campaigns (4, 12, 15, 20, 33, 48, 68 and 104 days after the start of infiltration) were conducted to monitor the hydrogeochemical effects in the post hot water infiltration phase. In each monitoring campaign, water samples were taken from 40 to 70 monitoring points (3 to 5 per well). To minimise hydraulic effects of the sampling campaigns, groundwater samples from the 2-inch wells were retrieved with low pumping rates of ~4 L/min by submersible pumps (MP1, Grundfos GmbH, Erkrath, Germany; or Whale submersible electric galley pump, Munster Simms Engineering Ltd., Bangor, Northern Ireland). The water samples from the different screened depths in the 2-inch wells (7–8, 10–11 and 13–14 m bgs) were separated by using packers above and below the pump submerged to the respective monitoring depths. The water then flowed through a PVC tube into a mixing cell, where probes for the on-site parameters (see 2.4.) were installed. To pump groundwater from the CMT-wells into the mixing cell (~100 mL/min), peristaltic pumps, stainless steel capillaries and viton (pumping) tubes were utilised, which allowed to minimise intrusion of oxygen, despite a relatively long residence time in the pumping system. In both setups, water samples for the analytical vials (see 2.4.) were taken at a three-way-valve directly before the mixing cell. Keller et al. (2021) used several baseline and post hot water infiltration sampling campaigns to also take water samples for investigating the potential effects of elevated temperatures on the microbial diversity and total cell counts to mutually support data interpretation.

2.4. Analytics of aqueous samples

On-site parameters (pH, Eh, electrical conductivity and O_2 concentration), main cations, main anions, NPOC, total inorganic carbon (TIC; laboratory tests), ammonium and dissolved methane and trichloroethylene (TCE) were analysed using standard geochemical methods. Alkalinity was determined by acid titration. Trace element and heavy metal samples were filtered with 0.2 mm RC-filters and analysed by an inductively coupled plasma mass spectrometer (7500cs; Agilent Technologies, Inc., Santa Clara, CA, USA) following the method described in Garbe-Schönberg (1993) for the elements Li, Al, V, Cr, Co, Ni, Cu, Zn, As, Se, Sr, Mo, Cd, Sn, Sb, Ba, Tl, Pb and U.

2.5. Prediction of potential concentration changes in the hot water infiltration field test based on laboratory investigations

The concentration changes between the laboratory batch tests at 10, 40 and 70 °C were used to predict temperature-dependent potential concentration changes in the hot water infiltration field test. First, the component-specific relative concentration changes, between the batch tests at increased temperatures of 40 and 70 °C and the reference batch tests at 10 °C, were calculated for all 28 sediment samples and plotted against temperature (as shown for V in Fig. A.2). Relative changes were chosen over absolute values as they allow for better consideration of different base concentration levels. Then, the 0th, 25th, 50th, 75th and 100th percentile of the 28 component-specific relative concentration changes between 10 and 40 °C and 40 and 70 °C were approximated by linear or exponential regression functions. Whether linear or exponential regression functions were applied for a component was determined by the higher coefficient of determination for the median concentrations (50th percentile) over the whole temperature range (from 10, to 40 and 70 °C). The two temperature ranges were calculated separately to prevent over- or underestimations of concentrations around the temperatures actually investigated in the laboratory batch tests, while enabling the prediction of concentrations in between. To calculate well and depth-specific potential concentration changes, the corresponding baseline concentrations and temperature measurements completed the

equations (as shown in Eqs. A.1 and A.2).

This procedure resulted in a component-specific potential concentration range calculated from the heterogeneity of the sediment samples investigated in the laboratory batch tests, linked with the baseline concentrations and the temperatures measured in the hot water infiltration field test.

3. Results and discussion

3.1. Geochemical effects in laboratory experiments

Overall, temperature-induced geochemical effects in the laboratory tests followed the pattern expected from previous studies: for the main groundwater constituents, an increase in temperature caused a release of organic carbon (Brons et al., 1991; Jesußek et al., 2013a), silica and potassium (Arning et al., 2006; Holm et al., 1987), whereas concentrations of inorganic carbon, calcium and magnesium decreased (Griffioen and Appelo, 1993; Fig. 2a). Despite the elevated NPOC concentrations, microbial catalysed redox reactions appeared to be limited within the one-week sediment-water contact time, as expected from lag phases of microbial growth (Mellefont and Ross, 2003). This resulted in negligible effects on median concentrations of redox sensitive parameters, such as nitrate and sulphate. Also, the median concentrations of trace elements and heavy metals mostly behaved as expected from the literature: increasing concentrations with increasing temperature were observed for monovalent cations (Li and Tl) and those components likely present as oxyanions (e.g. V, As, Se and Mo). Concentrations of divalent cations (e.g. Co, Ni and Zn) rather decreased (M. Bonte et al., 2013b; Lüders et al., 2020; Fig. 2b). Unlike afore cited studies, concentrations of Cu and Al increased in several sediment samples at 70 °C.

Most of the components, which showed elevated concentrations at increased temperatures, also demonstrated a greater concentration variation at 40 and even more at 70 °C, compared to 10 °C (e.g. Si_{diss}, Li, V, Cr, As, Se and Sb). A similar wider scattering of concentrations at higher temperatures has also been reported by M. Bonte et al. (2013b) and Lüders et al. (2020). Taken together, the small-scale heterogeneity in groundwater chemistry at ambient temperatures observed in the baseline monitoring for the hot water infiltration test (Fig. 4, Fig. A.1), can be expected to increase when temperatures rise. This would result in, not only shifted, but also wider concentration ranges at elevated temperatures.

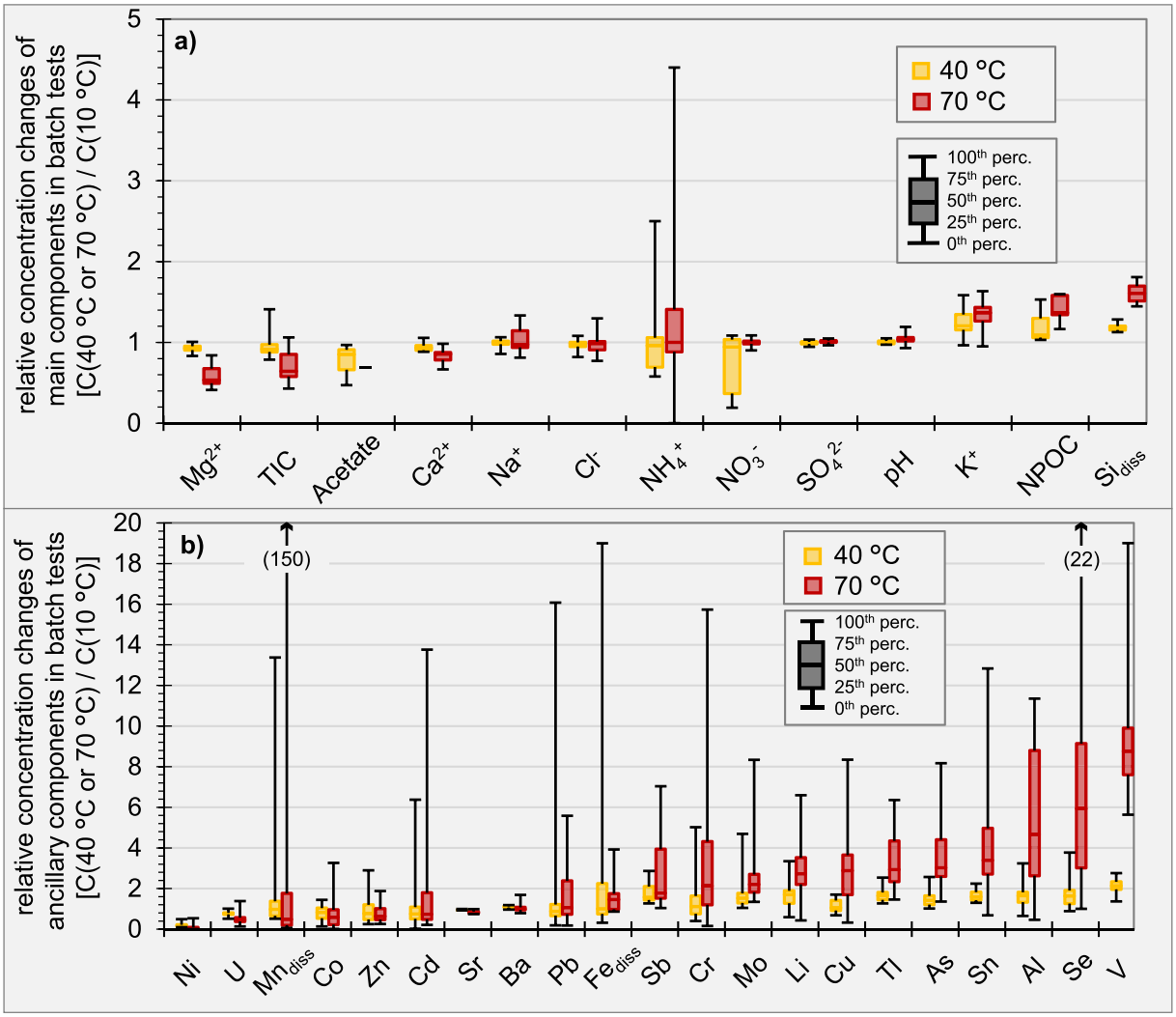

Fig. 2. Impact of temperature on concentrations of main (a) and ancillary (b) groundwater components in one-week batch tests at 10, 40 and 70 °C. Shown are the 0th, 25th, 50th, 75th and 100th percentile of relative concentration changes at 40 and 70 °C compared to those at 10 °C from the 28 sediment samples; sorted from the strongest relative decrease in median concentrations between 10 and 70 °C on the left towards the respective strongest increase on the right.

3.2. Effects of the hot-water infiltration field test on aquifer hydrochemistry

3.2.1. Temporal evolution of induced temperature changes

The infiltration of the hot water caused elevated temperatures, up to ~70 °C in close proximity to the infiltration well. Higher temperatures at the top of the aquifer than at the bottom (Fig. 3) can be attributed to temperature induced vertical convection, as shown by coupled numerical simulations (Heldt et al., 2021), with local variations in hydraulic permeability (see HPT-logs in Fig. 1) contributing to spatial variations. Around the first monitoring campaign, 4–5 days after the start of the hot water infiltration, maximal temperatures of 72 °C were recorded at the monitoring points 7.5 m bgs in wells C05 and D01, 1–1.5 m away from the infiltration well (see Fig. 1 for positions). In monitoring wells C04, C08, D03, D04 and D06, all 3–4 m away from the infiltration well, the highest temperatures (30–41 °C) at 7.5 m bgs were recorded around the second monitoring campaign, 12–13 days after infiltration start. The monitoring wells further downstream (D08, D09, D10; 6.5 m away from the infiltration well) showed the highest temperatures of 14–15 °C around the 5th and 6th monitoring campaigns, 48–68 days after the start of the infiltration. A more detailed insight into temporal and spatial evolution of temperatures is presented in Heldt et al. (2021).

3.2.2. Overview of geochemical effects induced by hot water infiltration

To determine the geochemical effects induced by the hot water infiltration, the average concentrations, including standard deviations, in wells around and downstream from the infiltration well were compared for the baseline period and the first (first month) and second (from second month onwards) post-infiltration periods. These average concentrations represent several monitoring wells and campaigns and, therefore, the effects of a mixture of reached temperatures. However, increased concentrations of NO_2^-, K^+, Si_{diss}, Li, V, Cr, As, Se, Mo, Sb, Ba, Tl, U and CH_4 during the post-infiltration period(s) can be attributed to the elevated temperatures as they exceeded the natural variations during baseline monitoring and the potential mixing effects of original and infiltrated water (Fig. 4). For all components, apart from NO_2^- and CH_4, which were not detected and U, which was not significantly affected, the trend of increasing concentration with increasing temperature is also apparent in the laboratory batch tests (Fig. 2). Conversely, not all expected concentration changes apparent in the batch tests (e.g. for Co) were obvious and distinguishable from water mixing in the field measurements. The decreasing Cl^- concentrations and increasing U concentrations in the field measurements (Fig. 4) do not fit the expectations based on the laboratory batch tests (Fig. 2) and cannot be fully explained by water mixing processes between original and infiltrated water and therefore, for now, must be attributed to an unidentified process. Beside the quantitatively limited concentration changes of NO_2^- and CH_4 (<15 μmol/L), there were no indications of an intensification of microbially catalysed redox processes in the field measurements. This fits with expectations, as elevated temperatures were sustained only for a couple of days, and is also supported by the observation of only minor temperature-induced changes in the microbial community (Keller et al., 2021).

3.2.3. Reversibility of concentration changes in the field test

In ATES systems, geochemical reversibility characterises how aquifer hydrogeochemistry affected by elevated temperatures returns to initial conditions when temperatures decrease: a) around/downstream of the "hot well" during hot water infiltration and the storage period; b) due to heat extraction between hot water recovery and water re-infiltration into the "cold well" and c) after termination of ATES operation. To investigate how far the geochemical effects of elevated temperatures persist, maximal concentrations of K^+, Si_{diss}, Li, V, As, Mo and Se, that all showed increased concentrations near the infiltration well, were observed downstream. With increasing distance from the infiltration well (T_{max} = 78 °C), maximal temperatures decreased from 73 to 41 °C and down to 15 °C at 1 m (D01), 3 m (D03) and 6.5 m (D09) from the well, respectively. Similar behaviour was observed for the maximal concentrations of Li, V, As, Mo and Se, as they returned to values within or near the geogenic range (Fig. 5). Thus, the field test data validated the rapid concentration changes with declining temperatures for components which concentration changes are related to temperature-dependent ion exchange and (de)sorption processes (e.g. Li, V, As, Mo and Se; Fig. 5) as has been shown in previous laboratory (Lüders et al., 2020) and modelling (Bonte et al., 2014) studies. As expected, reversal concentration changes related to mineral dissolution and precipitation (Si_{diss} and K^+) were slower.

In case of longer sustained elevated temperatures, induced reductive dissolution of Fe- and Mn (hydr)oxides may reduce sorption capacity and thus reversibility (Bonte et al., 2013a; Lüders et al., 2020). Oxidative dissolution to a relevant extent is unlikely in this field test, as the oxygen concentration of the infiltrated water (0.9 mg/L; Fig. 4) was below the median oxygen concentrations in all monitored depths in the baseline monitoring (Fig. A.1.), which also indicated a rather oxidised state of the sediment. However, in settings with larger oxygen infiltration, also oxidative dissolution reactions might play a role. Further, in a cyclic heat storage operation, groundwater constituents released at elevated temperatures will partly also be extracted with the hot water and fixated around the cold well after reinfiltration (as modelled by Bonte et al., 2014), or in potential mineral precipitates e.g. in the surface installations. Thus, the overall effect on the (re)distribution of released groundwater constituents is controlled by the interplay of the aforementioned processes and requires further research.

3.3. Direct comparison of concentrations between the laboratory batch tests and the field test

For a primary comparison of concentrations between the field and the laboratory data at high temperatures, the data from the batch tests at 70 °C and monitoring points sampled at temperatures >55 °C were directly compared (the comparison of data from monitoring points sampled between 25 and 55 °C and associated batch tests at 40 °C is in the supplementary information; Fig A.3). After the five-day hot water infiltration, five monitoring points, all from the central monitoring wells C05, C07 and D01 which are within a 1.5 m radius around the infiltration well, fit this criterion.

The maximal concentrations of components in the field samples >55 °C were within or below the concentration range of the laboratory batch tests at 70 °C for 24 of 31 components (all but NPOC, TIC, NO_3^-, Si_{diss}, Co, Ba and Tl). Overall, environmentally relevant concentration increases of most ancillary components seemed to be well represented. Moreover, despite the larger temperature range of the field samples (59–72 °C), the field data concentration range was smaller than the laboratory data concentration range for 26 of 31 components (all but NPOC, Co, Ni, Ba and Tl; Fig. 6). Both aspects are plausible, as the sediment samples investigated in the batch tests, originated from a wider area than the three central monitoring wells (Fig. 1). Thus, within the central hot zone around the infiltration well, the water may have only been in contact with a limited range of sedimentary compositions. Another possible explanation for this observation may also lie in the flow path of the water from the infiltration until the respective monitoring well; the water can encounter sediments of slightly different compositions, which potentially counterbalances the strongest effects. Both explanations indicate that considering a (preferably wide) variety of individual small-scale sediment samples in laboratory tests might serve as a safety buffer for concentrations expectable on the field scale.

3.4. Comparison of field concentrations with the predicted concentration range from laboratory batch tests

With focus on the initial concentration changes caused by the highest temperatures attained in the field test, the predictive power of the

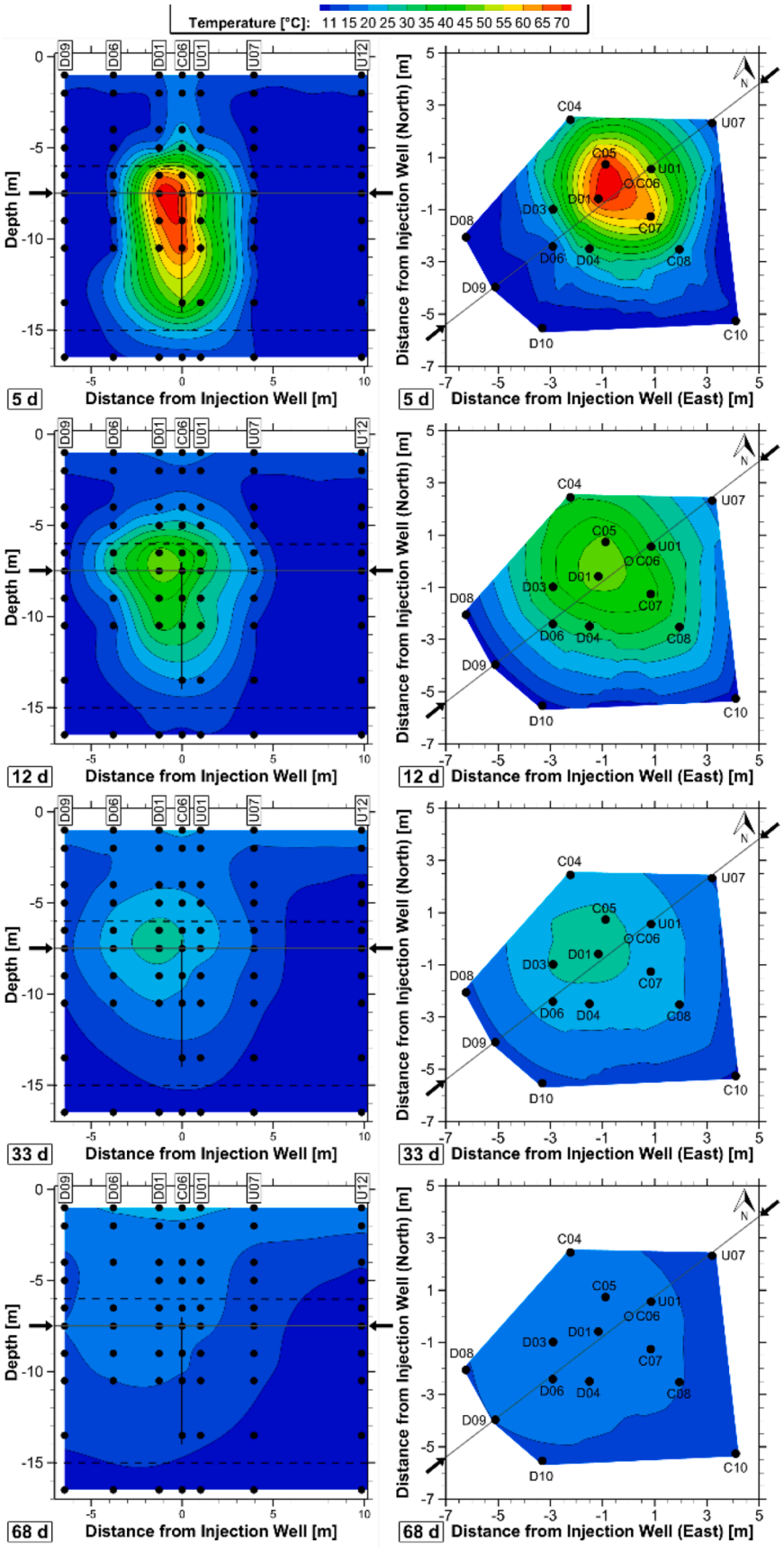

Fig. 3. Interpolated temperatures on a vertical (left column) and horizontal (right column) cross-section through the field test area at 5, 12, 33 and 68 days after start of the hot water infiltration (top to bottom rows). The vertical section is taken along the profile "FD (Flow Direction)" in Fig. 1, with groundwater flow from the top right to the lower left along the indicated profile. The horizontal section is shown for a depth of 7.5 m below ground surface, i. e. near the top of the aquifer. Black dots indicate temperature measuring points. The interpolated temperature distributions were derived by kriging using Tecplot 360 (Tecplot, Inc., WA, USA) with a range value of 0.3, a zero value of 0, a linear drift and taking into account the eight nearest points for the horizontal plane and all the points for the vertical cross section.

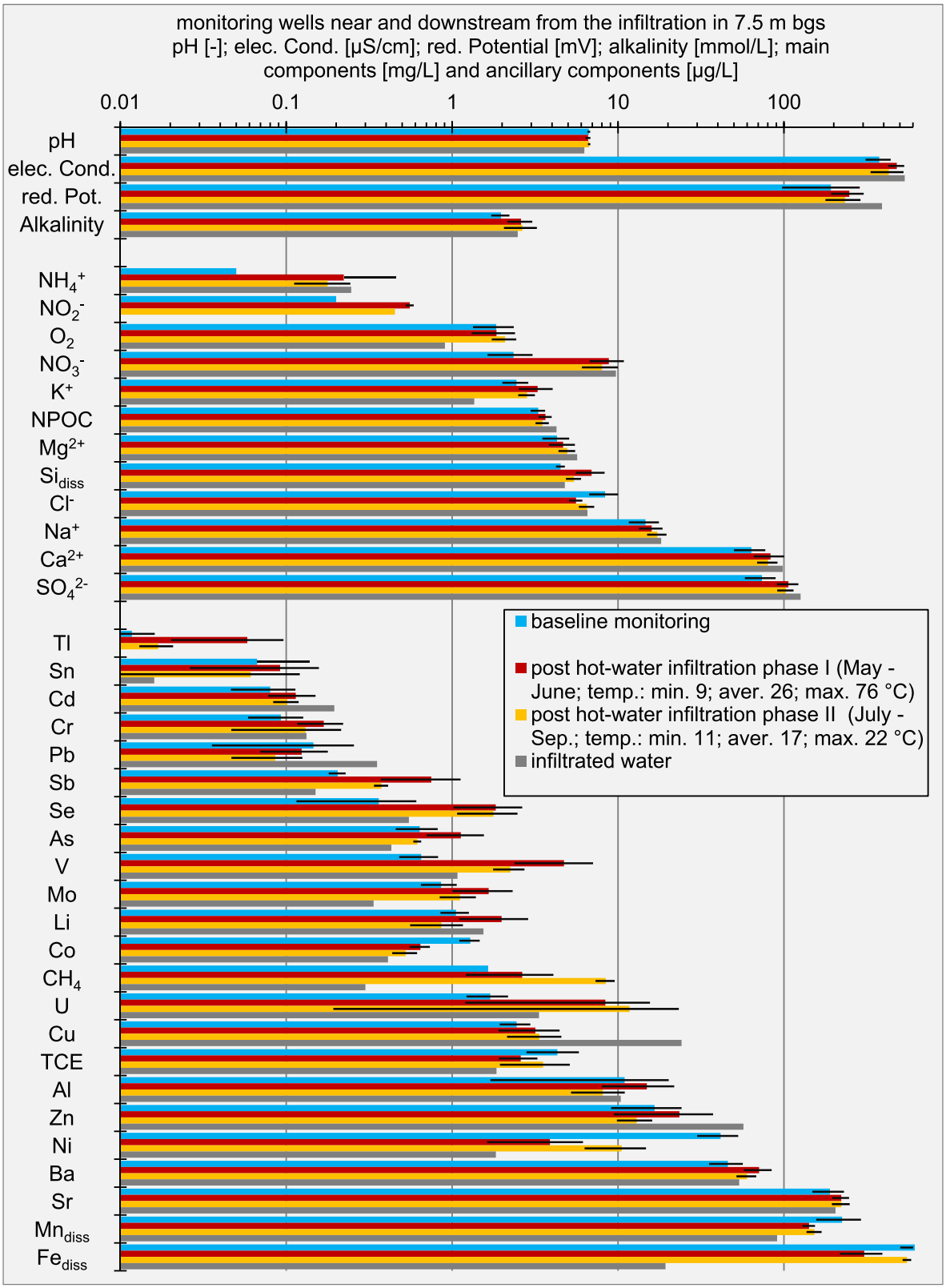

Fig. 4. Overview of field data for monitoring wells U01, C04, C05, C07, C08, D01, D03, D04, D06, D08, D09 and D10 (in 7.5 m below ground surface (bgs); see Fig. 1 for positions), separated after sampling during baseline monitoring, the first month after hot water infiltration, the further post infiltration phase and the infiltrated water. Average values and standard deviations are shown; main and ancillary components are sorted by ascending concentration, after the average baseline concentration within their group.

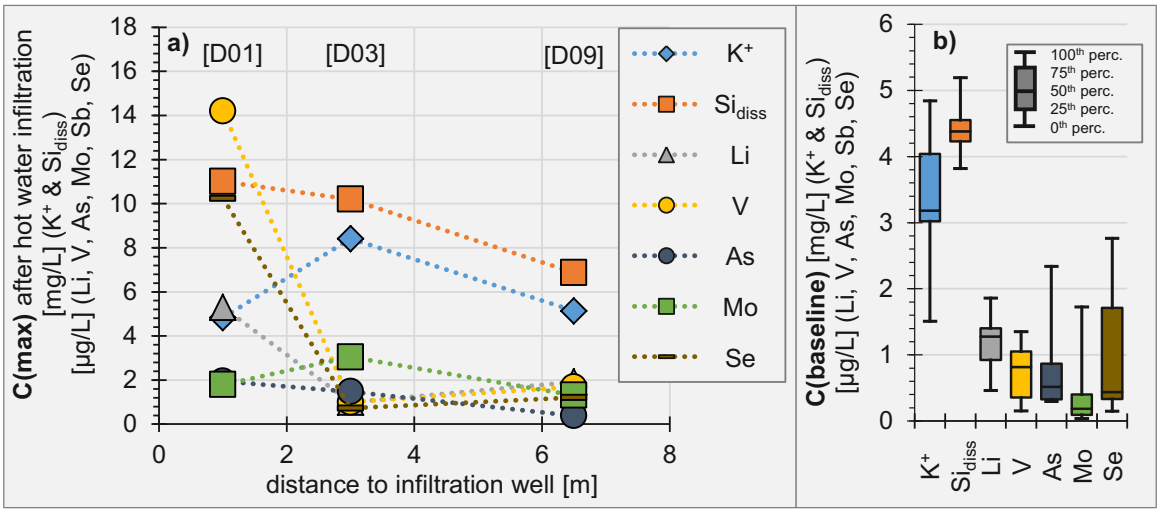

Fig. 5. Downstream development of K^{+}, Si_{diss}, Li, V, As, Mo and Se concentrations (a) that were increased due to hot water infiltration; compared to baseline concentrations in the respective monitoring wells D01, D03 & D09 (b).

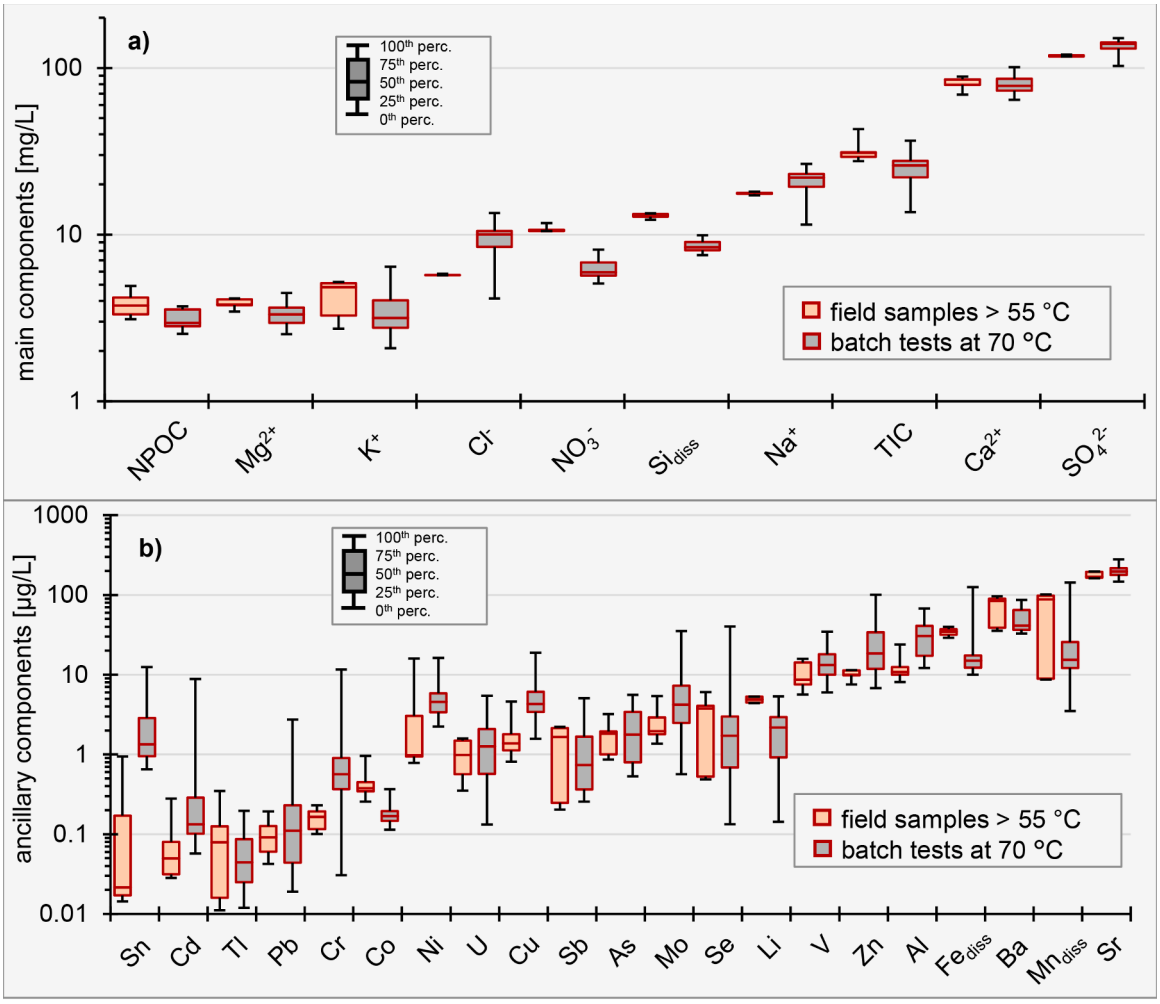

Fig. 6. Comparison of (a) main and (b) ancillary components concentrations in field samples from monitoring points C05 (7.5 and 10.5 m below ground surface [*bgs*]), C07 (7.5 bgs) and D01 (7.5 and 10.5 m bgs) in the temperature range 55 – 75 °C ($n = 5$) and the concentrations in samples from the 70 °C batch tests ($n = 28$). Components are sorted after median concentrations (50th percentile) in the field measurements; data for field samples in the temperature range from 25 to 55 °C ($n = 10$) in comparison to the batch tests at 40 °C ($n = 28$; Fig. A.3).

laboratory batch tests was evaluated temporally by the first monitoring campaign after hot water infiltration, and spatially by the three central monitoring wells nearest to the infiltration well (C05, C07 and D01; each with three sampled depths). Overall, 33% and 68% of the concentrations of main and ancillary groundwater components measured in these wells, respectively, were between the 0th and 100th percentile of the predicted concentration range based on the temperature-induced concentration changes in the laboratory batch tests (Fig. 7; see Fig. A.2 for explanation). With 43% and 40% of concentrations of main and ancillary components laying below the 50th percentile, respectively, there appeared to be a slight overall underestimation of concentrations by the laboratory-based predictions.

To determine whether the temperature during monitoring had an effect on the agreement between measured concentrations and the predicted concentration range, the comparison between measured and predicted concentrations was broken down to the individual monitoring points of the wells C05, C07, D01 and D03 ($n = 12$) including their respective sampling temperatures. Thereby, the overall accordance between measured and predicted concentrations was greatest, where the hot infiltrated water had cooled least prior to monitoring (Fig. 8a). The laboratory batch tests yielded the best results, in terms of predictive power, when the hottest temperature, and thus the largest change in concentration occurred, suggesting that the target infiltration temperature could be utilised as a basis for predicting the maximal expected temperature-induced concentration changes. On the on hand, maximal expectable concentration changes could be used as input parameters for scenario calculation that estimate the attenuated concentration changes in the wider surroundings (as e.g. shown in Lüders et al., 2020). On the other hand, the maximal expectable concentrations of environmentally relevant groundwater components are important for administrative approval procedures.

Furthermore, components with increased concentrations at elevated temperatures (K^+, Si_{diss}, Li, V, Cr, As, Se, Mo, Sb, Ba, Tl and U) also had a higher proportion of concentrations above the 100th percentile of predicted concentrations the further temperatures declined (Fig. 8b) which implies a retarded adaption of concentrations to decreasing temperatures.

Despite the similar trend for main and ancillary components, there is a significant gap in the accordance between these groups (Fig. 8a), indicating different behaviour of individual (groups of) components. To address this, the underlying data of Fig. 7 was broken down to the individual groundwater constituents (Fig. 9). From the main groundwater components, the measured concentrations of Mg^{2+}, TIC, Ca^{2+}, NO_3^-, Na^+, K^+, Cl^-, SO_4^{2-} and Si_{diss} were within the predicted concentration range for less than 50% of the monitoring wells C05, C07 and D01. Considering the data in Figs. 2, 4 and 6, three distinct groups of these components can be identified. For Na^+, Cl^-, NO_3^- and SO_4^{2-} with comparatively small temperature-dependent concentration changes in the laboratory batch tests (Fig. 2), concentration changes due to mixing of infiltrated water (Fig. 4) with residual water from around the infiltration well probably exceeded any potential temperature-related concentration changes. Concentrations of TIC, Ca^{2+}, Mg^{2+} and Sr that were predominantly affected by temperature-dependent precipitation of carbonates (Griffioen and Appelo, 1993; Reddy and Nancollas, 1976) behave differently: to reach the target infiltration temperatures of 75 to 80 °C, temperatures in the surface installations (heat exchanger, tubes and tanks) must be even higher, and reached temperatures between 80 and 90 °C. This had no impact on geochemical processes that demand sediment-water contact, though mineral precipitation processes related to elevated temperatures can be affected. Therefore, the higher temperatures before infiltration probably caused stronger carbonate precipitation than expected based on the logged in-aquifer temperatures, which is not considered in the predicted concentration range calculations. Concentrations of TIC, Ca^{2+} and Mg^{2+} in the extracted water (Table 2) deviated from the values around the infiltration well in the baseline monitoring (Fig. 4; Fig. A.1), adding the mixing of the different waters as an additional source of uncertainty. Si_{diss}, Tl and, to a lesser extent K^+, showed increasing concentrations at elevated temperatures in the laboratory batch tests (Fig. 2), that were also visible in the field data (Fig. 4). However, the Si_{diss} and K^+ concentrations declined slower than other components when temperatures decreased (Fig. 5), and Si_{diss} concentrations measured in the monitoring wells exceeded those observed in the laboratory tests (Fig. 6). The conducted batch tests seem to slightly underestimate concentration changes for silica, potassium and thallium (substituting potassium in silicates; Shaw, 1952), which is probably related to mineral dissolution of potassium bearing silicates and amorphous silica being the underlying release processes (Arning et al., 2006; M. Bonte et al., 2013b).

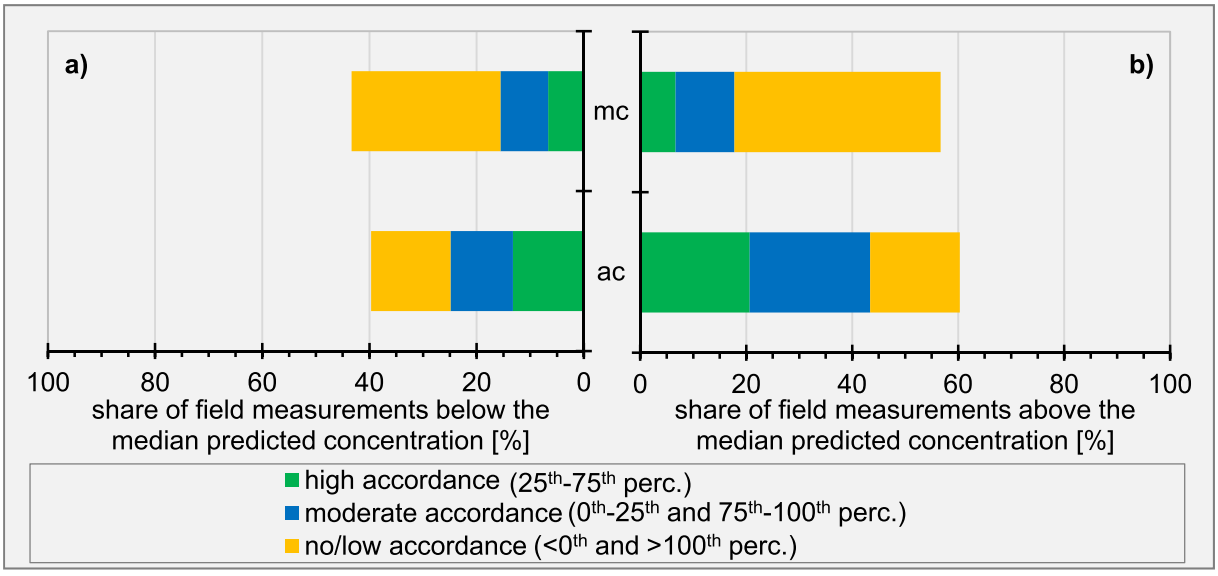

Fig. 7. Average accordance of main (mc) and ancillary components (ac) concentrations measured in wells C05, C07 and D01 during the first monitoring campaign after the hot water infiltration, with the predicted concentrations based on the temperature-induced concentration changes in the laboratory batch tests. The shares of field measurements (a) below and (b) above the median predicted concentrations are shown, separated for the intervals below, between and above the 0th, 25th, 50th, 75th and 100th percentile of predicted concentrations on the respective side of the figure.

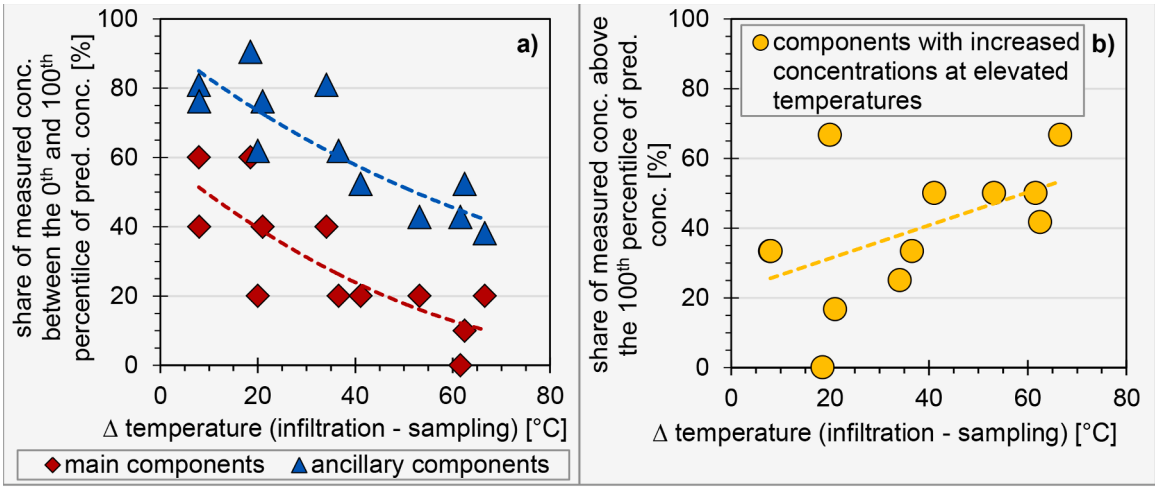

Fig. 8. (a) Share of main and ancillary components concentrations measured at 7.5, 10.5 and 13.5 m below ground surface (bgs) in wells C05, C07, D01 and D03 that were between the 0th and the 100th percentile of predicted concentrations; and (b) share of concentration of components with increased concentrations at elevated temperatures (see 3.2.2.) measured at 7.5, 10.5 and 13.5 m bgs in wells C05, C07, D01 and D03 that were above the 100th percentile of predicted concentrations; in relation to both the temperature deviation between infiltrated water and the temperature of the monitoring well during sampling in the respective depth. Data were taken from the monitoring campaign after the hot water infiltration with the highest temperatures (first campaign for C05, C07 and D01; second for D03).

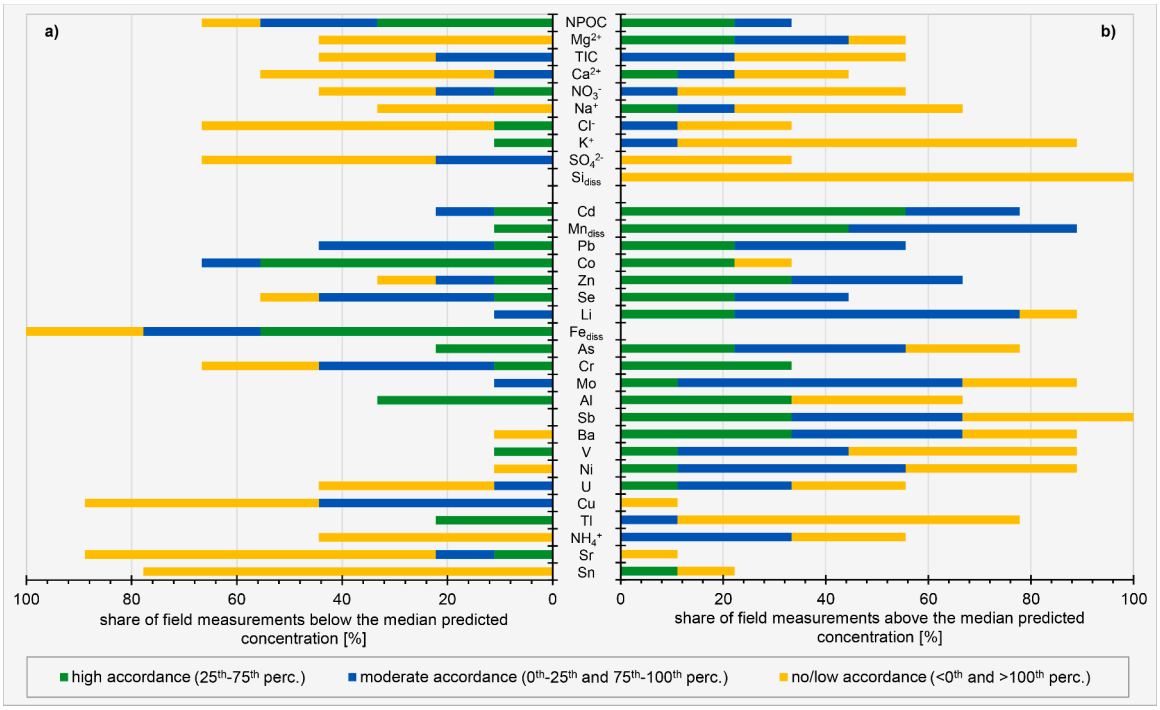

Fig. 9. Average component specific accordance of concentrations measured in wells C05, C07 and D01 during the first monitoring campaign after the hot water infiltration with the predicted concentrations based on the temperature induced concentration changes in the laboratory batch tests. Shown are the shares of field measurements (a) below and (b) above the median predicted concentrations, separated for the intervals below, between and above the 0th, 25th, 50th, 75th and 100th percentile of predicted concentrations on the respective figure side.

Overall, ancillary components showed a better agreement between measured and predicted concentrations than the main components. Ion exchange is the controlling process for most ancillary components (M. Bonte et al., 2013b; Lüders et al., 2020); therefore, their temperature-induced concentration changes are apparently more directly affected by elevated temperatures, and relatively less by auxiliary effects, such as water mixing, mineral precipitation and dissolution. However, the concentrations of the ancillary components measured in the monitoring wells C05, C07 and D01 that were within the predicted concentration ranges to more than 50% (from Cd to Ni in Fig. 9), were rather in the upper range (50th to 100th percentile) of predicted concentrations (Fig. 9). This indicates a slight underestimation of their concentration changes by the conducted batch tests. U, Cu, Tl, NH_4^+, Sr and Sn showed an accordance between measured and predicted concentrations of less than 50% for the referred monitoring wells (Fig. 9). In contrast to most other component concentrations, U, Cu, NH_4^+ and Sn were changing erratically, rather than gradually over time, starting from the baseline monitoring. Thus, the actual effect of elevated temperatures on concentrations of these components, as well as their predictability, remains uncertain.

4. Conclusions

A short-term hot water infiltration field test for simulating the hydrogeochemical effects caused by an initial heating phase of a HT-ATES system led to temperatures above 70 °C near the infiltration well. Frequent sampling of 17 monitoring wells tracked hydrochemical changes with high spatial and temporal resolution, enabling an evaluation of the predictive power of laboratory batch tests, conducted with 28 individual sediment samples from the field test site at 10, 40 and 70 °C.

In monitoring wells around the hot-water infiltration well, elevated temperatures caused increased concentrations of NO_2^-, K^+, Si_{diss}, Li, V, Cr, As, Se, Mo, Sb, Ba, Tl, U and CH_4. Changes in other groundwater constituents were either indistinguishable from the concentration range observed during baseline monitoring or from mixing effects of infiltrated and original water (O_2, NPOC, NH_4^+, NO_3^-, SO_4^{2-}, Na^+, Mg^{2+}, Ca^{2+}, Fe_{diss}, Mn_{diss}, Al, Co, Ni, Cu, Zn, Sr, Cd, Sn, Pb and TCE). A direct comparison with the laboratory batch test data identified the following:

- the trend of increasing concentrations with increasing temperature in the field measurements of the aforementioned components, except for NO_2^-, CH_4 and U, is as predicted by the laboratory batch tests.
- conversely, not all concentration changes expected from the batch tests were observed in the field measurements, partly due to superimposition by water mixing in the field.
- the maximal concentrations in field measurements above 55 °C were within or below the concentration range in the laboratory batch tests at 70 °C, for 24 out of 31 components (all but NPOC, TIC, NO_3^-, Si_{diss}, Co, Ba and Tl).

Furthermore, for 26 out of 31 viewed components the concentration ranges in the batch tests at 70 °C were larger than the concentration ranges measured in the five monitoring points sampled at temperatures above 55 °C. For this field test site, the concentration changes observed in the laboratory tests were attenuated at the field scale.

A comparison of field measurements from the three central monitoring wells C05, C07 and D01 with predicted concentration ranges based on the temperature-induced relative concentration changes in the laboratory batch tests revealed the following:

- overall agreement of field measurements with the predicted concentration ranges is better for components that showed pronounced temperature-induced concentration changes related to ion exchange and (de)sorption processes (which is true for most environmentally relevant ancillary groundwater components).
- the conducted batch tests are less suitable for predicting temperature-induced concentration changes related to mineral dissolution.
- the accordance of the field measurements with predicted concentration ranges is greatest, where the least cooling between the hot water infiltration and the sampling occurred, indicating:
  - a retarded adaption of concentrations to decreasing temperatures.
  - that the maximal temperature-induced concentration changes of many ancillary components can be well predicted.
  - that the target infiltration temperature of the hot water can be used to estimate maximal expectable concentration changes.

This procedure, for component-specific predictions of potential concentration changes induced by elevated temperatures, is suitable for components related to ion exchange and (de)sorption processes in the vicinity of a hot water infiltration. Thus, utilising the maximal expected temperatures allows prediction of maximal expectable concentration changes for most of the environmentally relevant ancillary groundwater components. However, as temperatures decline with distance to the infiltration well, most of the surrounding aquifer will only be exposed to attenuated concentration changes. Both aspects will play a major role in authorisation procedures, from a geochemical point of view.

Successive shifts in the redox state towards stronger reducing conditions and associated concentration changes in redox sensitive components, as expected from prolonged high subsurface temperatures, and their predictability at the field scale, were not investigated here. The same applies for cyclic operation, apart from the initial heating phase, simulating the operating phase of a subsurface heat storage and its induced (bio)geochemical effects. Thus, both aspects are in focus of consecutive investigations. Finally, predicting the geochemically affected space around ATES systems also requires future association of laboratory data characterising potentially delayed or incomplete reversibility of heat-induced concentration changes with the evolution of temperatures at the field scale.

Funding

This study is part of the TestUM-Aquifer project funded by the German Federal Ministry of Education and Research (03G0875A), which had no role in study design; the collection, analysis and interpretation of data; in writing of the report; and in the decision to submit the article for publication.

Declaration of Competing Interest

The authors declare that they have no known competing financial interests or personal relationships that could have appeared to influence the work reported in this paper.

Acknowledgments

We thank our colleagues Markus Ebert and Frank Dethlefsen for their cooperation, improvements in analytics and valuable comments throughout the preparation of this study as well as Marco Mahnecke, Jens Wemhöner, Lena-Sophie Kuhr, Jan Gustmann, Nina-Sophie Keller and all other helping hands for supporting the field and/or laboratory investigations. Furthermore, we thank the project partners from UFZ-MET for geophysical exploration and installation of the monitoring wells, the ICP-MS laboratory at Kiel University's Institute of Geosciences for conducting the analysis of trace elements and heavy metals on the basis of scientific cooperation, as well as the municipality of Wittstock/Dosse and the Brandenburgische Boden GmbH for supporting the project. In addition, we would like to mention the Angus-projects (https://www.angus-projekt.de/de?set_language=en), in which the experimental basis for the here presented study was laid. Finally, we thank the two anonymous reviewers for their constructive comments that helped to improve the quality of this paper.

Supplementary materials

Supplementary material associated with this article can be found, in the online version, at doi:10.1016/j.wroa.2021.100121.

References

Andersson, O., 1990. Scaling and corrosion in subsurface thermal energy storage systems, in: Hooghart, J.C., Posthumus, C.W.S. (Eds.), Hydrochemistry and Energy Storage in Aquifers. pp. 53–71.

Arning, E., Kölling, M., Schulz, H.D., Panteleit, B., Reichling, J., 2006. Einfluss oberflächennaher Wärmegewinnung auf geochemische Prozesse im Grundwasserleiter. Grundwasser 11, 27–39. https://doi.org/10.1007/s00767-006-0116-0.

Bauer, S., Beyer, C., Dethlefsen, F., Dietrich, P., Duttmann, R., Ebert, M., Feeser, V., Görke, U., Köber, R., Kolditz, O., Rabbel, W., Schanz, T., Schäfer, D., Würdemann, H., Dahmke, A., 2013. Impacts of the use of the geological subsurface for energy storage: an investigation concept. Environ. Earth Sci. 70, 3935–3943. https://doi.org/10.1007/s12665-013-2883-0.

Bonte, M., Röling, W.F.M., Zaura, E., Van Der Wielen, P.W.J.J., Stuyfzand, P.J., Van Breukelen, B.M., 2013a. Impacts of shallow geothermal energy production on redox

processes and microbial communities. Environ. Sci. Technol. 47, 14476–14484. https://doi.org/10.1021/es4030244.
Bonte, M., Stuyfzand, P.J., Breukelen, B.M.Van, 2014. Reactive Transport Modeling of Thermal Column Experiments to Investigate the Impacts of Aquifer Thermal Energy Storage on Groundwater Quality. Environ. Sci. Technol. 48, 12099–12107. https://doi.org/10.1021/es502477m.
Bonte, M., Stuyfzand, P.J., Hulsmann, A., Van Beelen, P., 2011. Underground Thermal Energy Storage : environmental Risks and Policy Developments in the Netherlands and European Union. Ecol. Soc. 16, 22.
Bonte, M., van Breukelen, B.M., Stuyfzand, P.J., 2013b. Temperature-induced impacts on groundwater quality and arsenic mobility in anoxic aquifer sediments used for both drinking water and shallow geothermal energy production. Water Res 47, 5088–5100. https://doi.org/10.1016/j.watres.2013.05.049.
Brons, H.J., Griffioen, J., Appelo, C.a.J., Zehnder, a.J.B., 1991. Bio)geochemical reactions in aquifer material from a thermal energy storage site. Water Res 25, 729–736. https://doi.org/10.1016/0043-1354(91)90048-U.
EPA, 1997. U.S. Environmental Protection Agency. Superfund Innovative Technology Evaluation Program - Final Demonstration Plan For the Evaluation of Soil Sampling and Soil Gas Sampling Technologies. US EPA Archive Document.
Fleuchaus, P., Schüppler, S., Bloemendal, M., Guglielmetti, L., Opel, O., Blum, P., 2020. Risk analysis of High-Temperature Aquifer Thermal Energy Storage (HT-ATES). Renew. Sustain. Energy Rev. 133, 110153 https://doi.org/10.1016/j.rser.2020.110153.
Garbe-Schönberg, C.-.D., 1993. Simultaneous Determination of Thirty-Seven Trace Elements in Twenty-Eight International Rock Standards By ICP-MS. Geostand. Geoanalytical Res. 17, 81–97. https://doi.org/10.1111/j.1751-908X.1993.tb00122.x.
García-Gil, A., Epting, J., Garrido, E., Vázquez-Suñé, E., Lázaro, J.M., Navarro, J.Á.S., Huggenberger, P., Calvo, M.Á.M., 2016. A city scale study on the effects of intensive groundwater heat pump systems on heavy metal contents in groundwater. Sci. Total Environ. 572, 1047–1058. https://doi.org/10.1016/j.scitotenv.2016.08.010.
Griffioen, J., Appelo, C.A.J., 1993. Nature and extent of carbonate precipitation during aquifer thermal energy storage. Appl. Geochem. 8, 161–176. https://doi.org/10.1016/0883-2927(93)90032-C.
Gunnarsson, I., Arnórsson, S., 2005. Impact of silica scaling on the efficiency of heat extraction from high-temperature geothermal fluids. Geothermics 34, 320–329. https://doi.org/10.1016/j.geothermics.2005.02.002.
Hähnlein, S., Bayer, P., Ferguson, G., Blum, P., 2013. Sustainability and policy for the thermal use of shallow geothermal energy. Energy Policy 59, 914–925. https://doi.org/10.1016/j.enpol.2013.04.040.
Heldt, S., Wang, B., Hu, L., Hornbruch, G., Lüders, K., Werban, U., Bauer, S., 2021. Numerical Investigation of a High Temperature Heat Injection Test. J. Hydrol. 126229 https://doi.org/10.1016/j.jhydrol.2021.126229.
Henning, H.-.M., Palzer, A., 2012. 100% Erneuerbare Energien für Strom und Wärme in Deutschland. Fraunhofer-Institut für Solare Energiesysteme, ISE. Freiburg.
Heron, G., Crouzet, C., Bourg, A.C.M., Christensen, T.H., 1994. Speciation of Fe(II) and Fe(III) in Contaminated Aquifer Sediments Using Chemical Extraction Techniques. Environ. Sci. Technol. 28, 1698–1705. https://doi.org/10.1021/es00058a023.
Holm, T.R., Eisenreich, S.J., Rosenberg, H.L., Holm, N.P., 1987. Groundwater Geochemistry of Short-Term Aquifer Thermal Energy Storage Test Cycles. Water Resour. Res. 23, 1005–1019.
Jenne, E.A., Andersson, O., Willemsen, A., 1992. Well, Hydrology, and Geochemistry Problems Encountered in ATES Systems and Their Solutions. In: Jenne, E.A. (Ed.), Aquifer Thermal Energy (Heat and Chill) Storage: Proceedings of the 27th Intersociety Energy Conversion Engineering Conference. San Diego, CA. https://doi.org/10.4271/929153.
Jesußek, A., Grandel, S., Dahmke, A., 2013a. Impacts of subsurface heat storage on aquifer hydrogeochemistry. Environ. Earth Sci. 69, 1999–2012. https://doi.org/10.1007/s12665-012-2037-9.
Jesußek, A., Köber, R., Grandel, S., Dahmke, A., 2013b. Aquifer heat storage: sulphate reduction with acetate at increased temperatures. Environ. Earth Sci. 69, 1763–1771. https://doi.org/10.1007/s12665-012-2009-0.
Keller, N.S., Hornbruch, G., Lüders, K., Werban, U., Vogt, C., Kallies, R., Dahmke, A., Richnow, H.H., 2021. Monitoring of the effects of a temporally limited heat stress on microbial communities in a shallow aquifer. Sci. Total Environ. 146377 https://doi.org/10.1016/j.scitotenv.2021.146377.
Keon, N.E., Swartz, C.H., Brabander, D.J., Harvey, C., Hemond, H.F., 2001. Validation of an Arsenic Seqential Extraction Method for Evaluating Mobility in Sediments. Environ. Sci. Technol. 35, 2778–2784. https://doi.org/10.1021/es001511o.
Koproch, N., Dahmke, A., Köber, R., 2019. The aqueous solubility of common organic groundwater contaminants as a function of temperature between 5 and 70°C. Chemosphere 217, 166–175. https://doi.org/10.1016/j.chemosphere.2018.10.153.
Leventhal, J., Taylor, C., 1990. Comparison of methods to determine degree of pyritization. Geochim. Cosmochim. Acta 54, 2621–2625. https://doi.org/10.1016/0016-7037(90)90249-K.
Lüders, K., Dahmke, A., Fiedler, M., Köber, R., 2020. Temperature influence on mobilisation and (re)fixation of trace elements and heavy metals in column tests with aquifer sediments from 10 to 70 °C. Water Res 169. https://doi.org/10.1016/j.watres.2019.115266.
Lüders, K., Firmbach, L., Ebert, M., Dahmke, A., Dietrich, P., Köber, R., 2016. Gas-phase formation during thermal energy storage in near-surface aquifers: experimental and modelling results. Environ. Earth Sci. 75 https://doi.org/10.1007/s12665-016-6181-5.
Mellefont, L.A., Ross, T., 2003. The effect of abrupt shifts in temperature on the lag phase duration of Escherichia coli and Klebsiella oxytoca. Int. J. Food Microbiol. 83, 295–305. https://doi.org/10.1016/S0168-1605(02)00378-1.
Men, J., Cheng, F., 2011. Biodegradation and growth characteristics of a toluene-degrading strain. African J. Biotechnol. 10, 13299–13306. https://doi.org/10.5897/AJB11.811.
Meier zu Beerentrup, K., Dahmke, A. (2021) Experimentelle Untersuchungen zu hydrochemischen Veränderungen im Porenwasser von pleistozänen Till-Sedimenten im Temperaturbereich von 10 bis 60 °C. Presentation at the Angus-Symposium 2021: Energiespeicher im geologischen Untergrund. Online, 17.06.2021.
Molz, F.J., Parr, A.D., Andersen, P.F., 1981. Thermal energy storage in a confined aquifer: second cycle. Water Resour. Res. 17, 641–645. https://doi.org/10.1029/WR017i003p00641.
Němeček, J., Steinová, J., Špánek, R., Pluhař, T., Pokorný, P., Najmanová, P., Knytl, V., Černík, M., 2018. Thermally enhanced in situ bioremediation of groundwater contaminated with chlorinated solvents – A field test. Sci. Total Environ. 622–623, 743–755. https://doi.org/10.1016/j.scitotenv.2017.12.047.
Opel, O., Eggerichs, T., Otte, T., Ruck, W.K.L., 2014. Monitoring of microbially mediated corrosion and scaling processes using redox potential measurements. Bioelectrochem 97, 137–144. https://doi.org/10.1016/j.bioelechem.2013.11.004.
Peter, A., Lamert, H., Beyer, M., Hornbruch, G., Heinrich, B., Schulz, A., Geistlinger, H., Schreiber, B., Dietrich, P., Werban, U., Vogt, C., Richnow, H.H., Großmann, J., Dahmke, A., 2012. Investigation of the geochemical impact of CO2 on shallow groundwater: design and implementation of a CO2 injection test in Northeast Germany. Environ. Earth Sci. 67, 335–349. https://doi.org/10.1007/s12665-012-1700-5.
Perlinger, J.A., Almendinger, J.E., Urban, N.R., Eisenreich, S.J., 1987. Groundwater geochemistry of aquifer thermal energy storage: long-term test cycle. Water Resour. Res. 23, 2215–2226. https://doi.org/10.1029/WR023i012p02215.
Possemiers, M., Huysmans, M., Batelaan, O., 2014. Influence of Aquifer Thermal Energy Storage on groundwater quality: a review illustrated by seven case studies from Belgium. J. Hydrol. Reg. Stud. 2, 20–34. https://doi.org/10.1016/j.ejrh.2014.08.001.
Reddy, M.M., Nancollas, G.H., 1976. The crystallization of calcium carbonate. IV. The effect of magnesium, strontium and sulfate ions. J. Cryst. Growth 35, 33–38. https://doi.org/10.1016/0022-0248(76)90240-2.
Saito, T., Hamamoto, S., Ueki, T., Ohkubo, S., Moldrup, P., Kawamoto, K., Komatsu, T., 2016. Temperature change affected groundwater quality in a confined marine aquifer during long-term heating and cooling. Water Res. 94, 120–127. https://doi.org/10.1016/j.watres.2016.01.043.
Schwardt, A., Dahmke, A., Köber, R., 2021. Henry's law constants of volatile organic compounds between 0 and 95°C – Data compilation and complementation in context of urban temperature increases of the subsurface. Chemosphere 272, 129858. https://doi.org/10.1016/j.chemosphere.2021.129858.
Shaw, D.M., 1952. The geochemistry of thallium. Geochim. Cosmochim. Acta 2, 118–154. https://doi.org/10.1016/0016-7037(52)90003-3.
Stookey, L.L., 1970. Ferrozine-A New Spectrophotometric Reagent for Iron. Anal. Chem. 42, 779–781. https://doi.org/10.1021/ac60289a016.
Ueckert, M., Baumann, T., 2019. Hydrochemical aspects of high-temperature aquifer storage in carbonaceous aquifers: evaluation of a field study. Geotherm. Energy 7, 4. https://doi.org/10.1186/s40517-019-0120-0.
Willemsen, A., 1990. Water treatment and environmental effects, in: Hooghart, J.C., Posthumus, C.W.S. (Eds.), Hydrochemistry and Energy Storage in Aquifers. pp. 105–124.
Zuurbier, K.G., Hartog, N., Valstar, J., Post, V.E.a, van Breukelen, B.M., 2013. The impact of low-temperature seasonal aquifer thermal energy storage (SATES) systems on chlorinated solvent contaminated groundwater: modeling of spreading and degradation. J. Contam. Hydrol. 147, 1–13. https://doi.org/10.1016/j.jconhyd.2013.01.002.